INTERFACE

rsif.royalsocietypublishing.org

Research

Cite this article: He D, Earn DJD. 2016 The cohort effect in childhood disease dynamics. *J. R. Soc. Interface* **13**: 20160156.
http://dx.doi.org/10.1098/rsif.2016.0156

Received: 22 February 2016
Accepted: 20 June 2016

Subject Category:
Life Sciences–Mathematics interface

Subject Areas:
biomathematics

Keywords:
childhood infectious diseases, measles, age structure, cohort entry, school terms

Author for correspondence:
Daihai He
e-mail: hedaihai@gmail.com

Electronic supplementary material is available at http://dx.doi.org/10.1098/rsif.2016.0156 or via http://rsif.royalsocietypublishing.org.

THE ROYAL SOCIETY PUBLISHING

The cohort effect in childhood disease dynamics

Daihai He[1] and David J. D. Earn[2]

[1]Department of Applied Mathematics, Hong Kong Polytechnic University, Hong Kong SAR, China
[2]Department of Mathematics and Statistics, McMaster University, Hamilton, Ontario, Canada L8S 4K1

The structure of school terms is well known to influence seasonality of transmission rates of childhood infectious diseases in industrialized countries. A less well-studied aspect of school calendars that influences disease dynamics is that all children enter school on the same day each year. Rather than a continuous inflow, there is a sudden increase in the number of susceptible individuals in schools at the start of the school year. Based on the standard susceptible–exposed–infectious–recovered (SEIR) model, we show that school cohort entry alone is sufficient to generate a biennial epidemic pattern, similar to many observed time series of measles incidence. In addition, cohort entry causes an annual decline in the effective transmission that is evident in observed time series, but not in models without the cohort effect. Including both cohort entry and school terms yields a model fit that is significantly closer to observed measles data than is obtained with either cohort entry or school terms alone (and just as good as that obtained with Schenzle's realistic age-structured model). Nevertheless, we find that the bifurcation structure of the periodically forced SEIR model is nearly identical, regardless of whether forcing arises from cohort entry, school terms and any combination of the two. Thus, while detailed time-series fits are substantially improved by including both cohort entry and school terms, the overall qualitative dynamic structure of the SEIR model appears to be insensitive to the origin of periodic forcing.

1. Introduction

Using transmission models to uncover the mechanisms behind observed infectious disease dynamics is a major goal of mathematical epidemiology [1,2]. In the context of recurrent epidemics of childhood diseases such as measles, chicken pox and whooping cough, a large body of research has indicated that seasonal changes in transmission rate are fundamentally important in determining the structure and periodicity of infectious disease time series [1,3–9].

The primary source of transmission seasonality for childhood diseases in industrialized countries appears to be the aggregation of children in schools, which are closed between terms and during summer holidays [3]. Indeed, even crude reconstructions of the transmission rate from incidence data show clear evidence of school term structure [10,11]. Other external influences, such as seasonality of births [12] or weather [13,14] may contribute, but are more difficult to detect (one study indicates that climatic changes affect interannual differences in measles incidence in the UK [15]).

The traditional susceptible–infectious–recovered (SIR) and susceptible–exposed–infectious–recovered (SEIR) modelling frameworks [1,16], including seasonal forcing of the transmission rate, have been used extensively to examine and explain the *qualitative* dynamics observed for a wide variety of infections in different places and times [4–6,9,17,18]. In addition, detailed *quantitative* reconstructions of seasonally varying transmission rates for childhood diseases have been achieved, either by extending the Fine and Clarkson method [9,10,19–22] or by using more statistically well-founded inference methods, e.g. (i) the 'time-series SIR' (TSIR) framework in which a discrete-time SIR model subject to additive and multiplicative noise is fitted [23], (ii) stochastic epidemic modelling frameworks in which the data are treated as a partially observed Markov process,

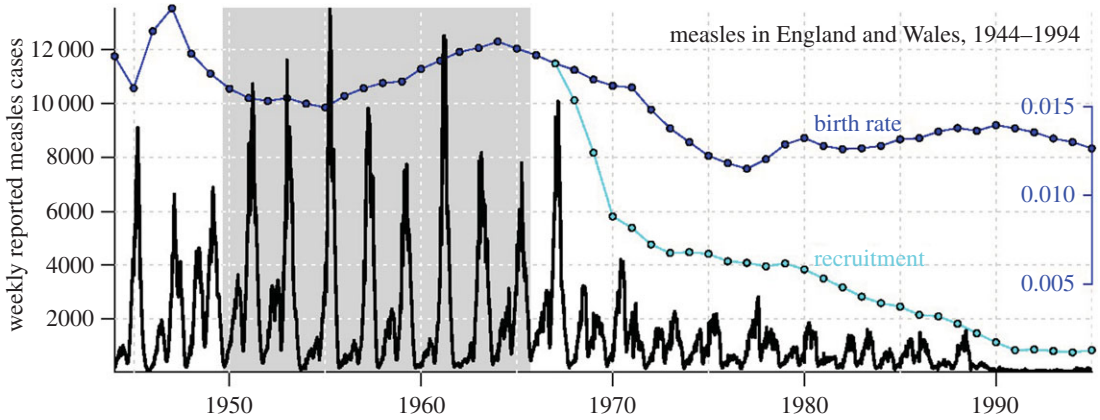

Figure 1. Weekly reported measles cases in 60 major cities of England and Wales, 1944–1994, with the biennial period studied by Fine & Clarkson [10] (8 September 1949 to 7 September 1965) highlighted in grey. The *per capita* annual birth rate and susceptible recruitment rate (birth rate adjusted to account for vaccination [5]) are shown in blue and cyan, respectively. (Online version in colour.)

fitted by particle filtering [24,25], or (iii) deterministic models fitted by generalized profiling, i.e. a combination of trajectory matching and gradient matching [7,26,27]. Other techniques are available for daily incidence data [28,29], but childhood disease incidence has typically been reported weekly.

Figure 1 shows the well-known time series of weekly reported measles incidence in 60 major cities of England and Wales (E&W), 1944–1994 [10,11,30–41]. The highlighted period from 1950 to 1964 displays a strictly biennial epidemic cycle, with large and small epidemics in alternate years. It is common to compare a biennial attractor of a deterministic epidemic model with this observed 2-year cycle [37,40,42,43]. Because such attractors are strictly periodic, the observed variation from biennium to biennium must be regarded as random fluctuations about the mean biennium. Figure 2*a* shows the average measles biennium with a dashed curve ($\pm$s.d. in grey). Figure 2*b* shows the transmission rate as reconstructed with the method of Fine & Clarkson [10].

The most obvious aspect of reconstructed childhood disease transmission rates such as that shown with a dashed curve in figure 2*b* is that they are high when school is in session and low otherwise [7,10,11], a feature that can easily be included in simple models using 'term-time forcing' [5,17,42]. Another clear aspect of reconstructed transmission rates is that they decline over the course of the school year [7,10], a feature that is not reproduced by the simple term-time forced SEIR model but is reproduced successfully by age-structured models that employ both term-time forcing and annual gradewise movement of school-age cohorts (figure 2, red points [37,40]).

We suggest that the most crucial element of the age-structured models—from the point of view of reproducing the aggregate temporal dynamics of childhood infections in industrialized countries—is the annual, sudden gradewise movement of age cohorts and, moreover, that the key aspect of gradewise movement is the sudden entry of the youngest school-age cohort into schools. This 'cohort effect' changes the way new susceptibles enter the system, i.e. each year some proportion of children effectively enter the well-mixed susceptible pool all at once on the first day of school, rather than continuously throughout the year as maternally acquired immunity wanes.

In E&W, the Education Act of 1944 [44] mandates that children must be in school from ages 5 to 16. In practice, this means that children enter school at age four or five.[1] The average age at which measles infection occurred in E&W during the period on which we focus was 4–5 years [1, p. 51], i.e. during the first year of school. Even the extreme approximation that *all* children entered the susceptible pool on the same day each year may be valid if pre-school children were usually infected by older siblings who were attending school.

In this paper, we show that incorporating the cohort effect in an epidemiological model is easy without introducing any explicit age structure, and that doing so yields an annual decline in the effective (reconstructed) transmission rate, as observed in real measles time series. Moreover, including the cohort effect yields simulation time series that fit observed disease incidence data more closely than standard term-time forced SEIR models. On the other hand, we find that the qualitative dynamic structure of the SEIR model is almost identical if seasonal forcing is implemented only in the transmission rate, only via the cohort effect, or any combination of the two. Consequently, the results of research aiming to understand transitions in the qualitative dynamics of childhood diseases (e.g. via bifurcations) appear to be robust to the detailed implementation of seasonality in the model.

The cohort entry model that we present here was first considered by He [45]. A stochastic version was included in a collection of models used to illustrate plug-and-play inference techniques by He *et al.* [25].

2. Methods

The standard SEIR model [1] can be expressed as a simple system of nonlinear ordinary differential equations

$$\frac{dS}{dt} = B - \beta SI - \mu S, \tag{2.1a}$$

$$\frac{dE}{dt} = \beta SI - \sigma E - \mu E, \tag{2.1b}$$

$$\frac{dI}{dt} = \sigma E - \gamma I - \mu I \tag{2.1c}$$

and

$$\frac{dR}{dt} = \gamma I - \mu R. \tag{2.1d}$$

Here, S, E, I and R denote the numbers of susceptible, exposed (infected but not yet infectious), infectious and recovered (immune) individuals. The parameters are the rates of birth (B), *per capita* death (μ), transmission (β), onset of infectiousness (σ)

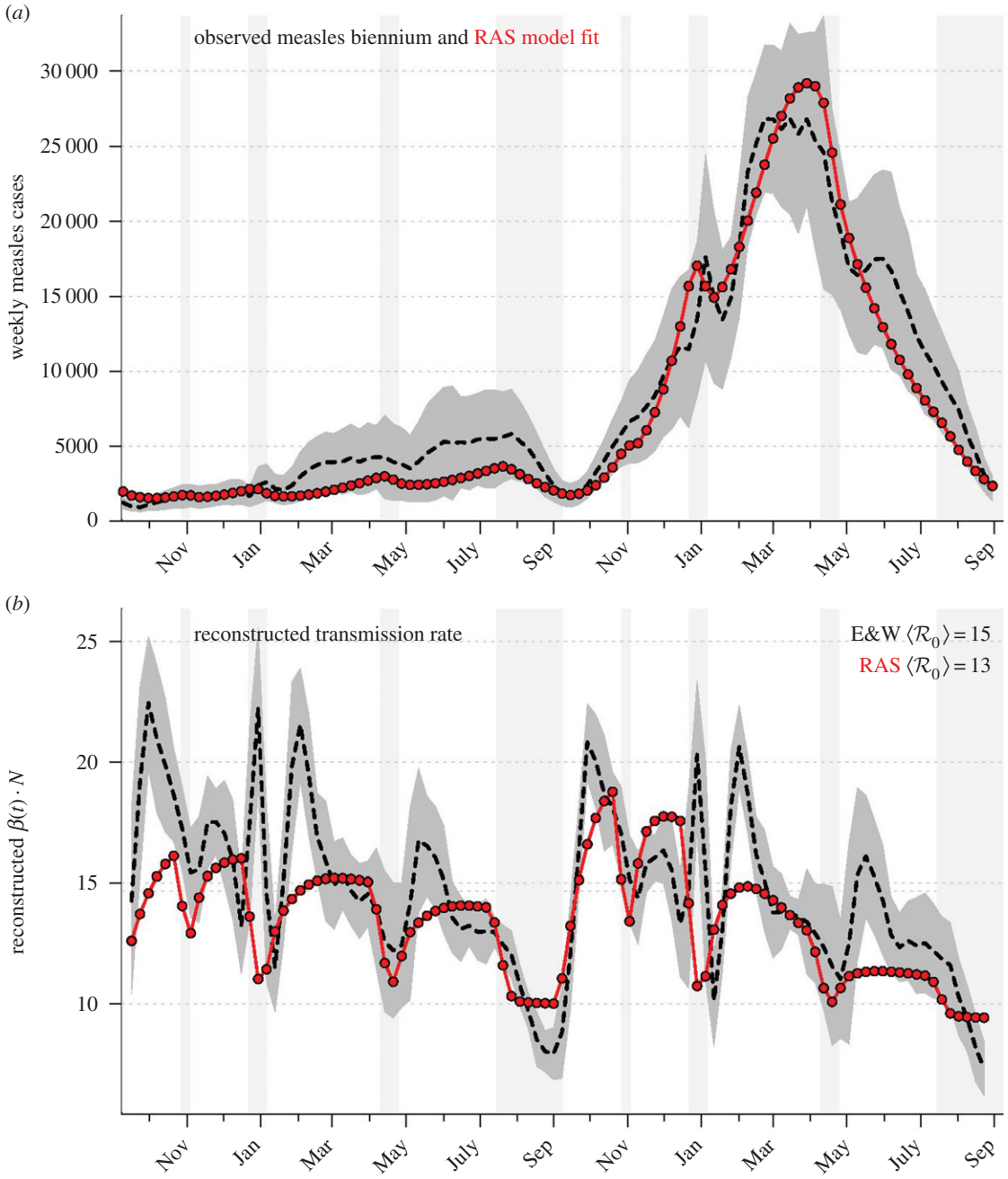

Figure 2. (*a*) Average biennial cycle of reported measles cases in England and Wales, 1950–1964. Mean (dashed) ± s.d. (grey). Best-fit biennial attractor of Schenzle's [37] realistic age-structured (RAS) model (red; see electronic supplementary material, §2). School vacations are indicated with light grey shading. (*b*) Transmission rate as reconstructed by the method of Fine & Clarkson [10] (see §2.3.5). Colour-coding as in panel (*a*). Transmission rate reconstructions from other models are shown in figure 3 and in the electronic supplementary material, figures S1 and S2. (Online version in colour.)

and recovery (γ). The mean latent and infectious periods are $\tau_E = 1/\sigma$ and $\tau_I = 1/\gamma$, respectively (for measles, $\tau_E \approx 8$ days and $\tau_I \approx 5$ days [1, p. 31]). The total population size is $N = S + E + I + R$. Disease-induced mortality is not included in equation (2.1) because it has a negligible population-level effect for typical childhood diseases [12]. Note that because equations (2.1*a*)–(2.1*c*) do not depend on the recovered class R, equation (2.1*d*) can be ignored.

The basic reproduction number $\mathcal{R}_0$ (the average number of secondary cases caused by a given primary case in a wholly susceptible population [1,2]) is ([8] and electronic supplementary material, equation (S8))

$$\mathcal{R}_0 = \frac{B}{\mu} \cdot \frac{\sigma}{\sigma + \mu} \cdot \frac{\beta}{\gamma + \mu}. \tag{2.2}$$

The first factor (B/μ) does not normally appear in formulae for $\mathcal{R}_0$ because it is usually assumed that $B = \mu N$ and N is usually absorbed into the transmission rate β. For measles in E&W during the period we examine, $\mathcal{R}_0 \approx 17$ [1, p. 70].

2.1. Seasonality of transmission rate

The transmission rate β is not constant for childhood infections. It varies seasonally as a result of the aggregation of children in schools [3]. The *term-time forced* transmission rate can be written [46]

$$\beta(t) = \langle\beta\rangle \begin{cases} 1 + 2(1 - p_s)\alpha & \text{school days} \\ 1 - 2p_s\alpha & \text{non-school days,} \end{cases} \tag{2.3}$$

where $\langle\beta\rangle$ is the mean transmission rate, α is the *amplitude* of forcing and p_s is the proportion of days on which school is in session. (Note that we always use $\langle \cdot \rangle$ to denote the time average of a quantity.)

2.2. The cohort effect

Early in life, most children have fewer social contacts than they do after entering school at age 4 or 5. This effective shielding from disease exposure is only partial, of course, and some young children become infected before entering school. For simplicity, we suppose that a proportion c of newborns is subject to the cohort effect, meaning complete shielding from disease transmission until entering school, whereas the remaining proportion $1-c$ enters the well-mixed population immediately after birth (or, in practice, after maternally acquired immunity wanes, which takes about four months in the case of measles [1]). We refer to the day of the year on which school begins as t_0 (e.g. if school starts on 8 September and we measure time in years, then $t_0 = 251/365 \simeq 0.688$). Thus, we implement the cohort effect in the model by replacing the constant annual birth rate B with the function

$$\widetilde{B}(t) = B\left((1-c) + c\sum_{k=0}^{\infty}\delta(t - t_0 - kL)\right), \tag{2.4}$$

where δ is the Dirac delta function and L is the length of the time interval between cohort entries (normally 1 year). The periodic forcing of the birth term specified in equation (2.4) affects $\mathcal{R}_0$ (which now depends on the time of year that initial invasion occurs [47]). Instability of the disease-free solution of this non-autonomous SEIR model is determined (approximately, but fairly accurately) by the condition $\bar{\mathcal{R}}_0 > 1$, where $\bar{\mathcal{R}}_0$ refers to the basic reproduction number of the autonomous system obtained by averaging the time-dependent parameters, i.e. using B rather than $\widetilde{B}(t)$ and replacing β by $\langle\beta\rangle$ in equation (2.2) [47–49].

2.3. Quantitative fits of models to observed time series

2.3.1. Observed measles time series

In the main text, we consider fits to the average biennium of the weekly measles reports in E&W from September 1949 to September 1963. In the electronic supplementary material, we repeat the analysis with three other (city level) measles time series that display a consistent biennial incidence pattern over a similar period:

(i) weekly reported measles in London, UK, from September 1949 to September 1965 (the same period fitted in [42,43]);
(ii) weekly reported measles in Liverpool, UK, from September 1945 to September 1965;
(iii) monthly reported measles in New York City (NYC), USA, from September 1945 to September 1963. To correct for the different lengths of each month in the NYC data, we followed [12] and multiplied each raw data point (reported measles in month j of year i) by

$$\frac{(\text{Days in year } i)/12}{\text{Days in month } j \text{ of year } i}. \tag{2.5}$$

2.3.2. Average measles biennium

The observed average biennial pattern (X_{obs}) and the variance about it (V_{obs}) can be written [42]

$$X_{\text{obs}}(t) = \frac{1}{k_{\max}}\sum_{k=0}^{k_{\max}-1}\hat{n}(t_0 + 2k + t), \quad 0 \le t < 2 \tag{2.6}$$

and

$$V_{\text{obs}}(t) = \frac{1}{k_{\max}-1}\sum_{k=0}^{k_{\max}-1}[\hat{n}(t_0 + 2k + t) - X_{\text{obs}}(t)]^2. \tag{2.7}$$

Here, $\hat{n}(t)$ refers to the number of notified (reported) measles cases at time t. We took the initial time to be $t_0 = 1949.688$ (8 September 1949) in E&W and London, and $t_0 = 1945.688$ (8 September 1945) in Liverpool and NYC. The number of biennia was $k_{\max} = 9$ in E&W, $k_{\max} = 10$ in London and NYC, and $k_{\max} = 12$ in Liverpool (see electronic supplementary material, figure S3 for the four time series).

2.3.3. Simulated measles incidence

To compare the models with the observed data, we solved the SEIR model (equation (2.1)) numerically with initial conditions taken to be a slight random perturbation of $(S(0), E(0), I(0)) = (1/\mathcal{R}_0, 10^{-4}, 10^{-4})$. After discarding a 500 year transient to ensure the solution had settled onto an attractor, we defined the simulated number of notified cases at report times t to be

$$n(t) = \int_{t-\Delta t}^{t}\eta \cdot N \cdot \gamma I(t)\,\mathrm{d}t, \tag{2.8}$$

where Δt is the notification interval (one week or one month), N is the population size (electronic supplementary material, table S1) and η is the *notification efficiency* (or *reporting ratio*) for measles [11,37] (electronic supplementary material, table S6). Because γI is the proportional rate at which individuals enter the recovered class (equation (2.1d)), it is a reasonable approximation of the rate at which cases are notified (before adjusting for population size and notification efficiency).

2.3.4. Best fit

Following Keeling & Grenfell [42], we found the parameters of a given deterministic model that yielded an attractor that best fits the observed biennium by minimizing the *weighted fitting error*

$$E_V(\boldsymbol{m}) = \frac{1}{2\text{yr}}\sum_{i=1}^{N_t}\frac{[X_{\text{obs}}(t_i) - n(t_i;\boldsymbol{m})]^2}{V_{\text{obs}}(t_i)}\Delta t. \tag{2.9}$$

Here, Δt is the reporting interval and N_t is the number of reporting intervals in a biennium (for weekly data, $\Delta t = 1/52$ year and $N_t = 104$). In equation (2.8), we used the notation $n(t)$ for the simulated number of cases at time t; here, we use the more cumbersome notation $n(t;\boldsymbol{m})$ to emphasize explicitly that the model solution depends on a vector $\boldsymbol{m}$ containing the N_p model parameters that are fitted (e.g. for the cohort-entry, term-time forced SEIR model, $\boldsymbol{m} = (\mathcal{R}_0, \eta, \alpha, c)$ and $N_p = 4$). E_V measures the total deviation of the model's attractor from the observed biennium, relative to the variation in the observed data [42]. Greater weight is given to points where the variation from biennium to biennium is smaller. All the noise in the data is implicitly assumed to arise from observation error as opposed to process error from intrinsic stochasticity.

E_V has a natural likelihood interpretation. Suppose the data point $\hat{n}_i$ observed at biennium time t_i is drawn from a distribution with probability density

$$d_i(\hat{n}, n(t_i;\boldsymbol{m});\boldsymbol{a}_i), \tag{2.10}$$

where $\boldsymbol{a}_i$ is a parameter vector associated with distribution d_i. Moreover, suppose that observations at different biennium times, $\{t_i : i = 1, \ldots, N_t\}$, are independent. Then, the likelihood of the model (specified by $\boldsymbol{m}$) given the data, i.e. the probability of obtaining the observed data given the model, is

$$\prod_{i=1}^{N_t}[d_i(\hat{n}_i, n(t_i;\boldsymbol{m});\boldsymbol{a}_i)\Delta t]. \tag{2.11}$$

If it is further assumed that the distributions d_i are normal, then

$$d_i(\hat{n}_i, n(t_i;\boldsymbol{m});\mu_i,\sigma_i^2) = \frac{1}{\sqrt{2\pi\sigma_i^2}}\exp\left(-\frac{1}{2\sigma_i^2}[\hat{n}_i - n(t_i;\boldsymbol{m})]^2\right). \tag{2.12}$$

where we have set $\mu_i = n(t_i; \boldsymbol{m})$. Now, taking $\hat{n}_i = X_{\text{obs}}(t_i)$ and $\sigma_i^2 = V_{\text{obs}}(t_i)$, the negative log likelihood is

$$-\mathcal{L} = \frac{1}{2}\sum_{i=1}^{N_t} \log(2\pi\sigma_i^2) + \sum_{i=1}^{N_t} \frac{[X_{\text{obs}}(t_i) - n(t_i; \boldsymbol{m})]^2}{2V_{\text{obs}}(t_i)^2} \quad (2.13a)$$

$$- N_t \log \Delta t$$

$$= \left(\frac{1\text{ yr}}{\Delta t}\right) E_V + \text{constant}, \quad (2.13b)$$

where the constant depends only on the data and not on the model parameters $\boldsymbol{m}$. Thus, E_V is a scaled and translated version of the negative log likelihood, and minimizing E_V yields a maximum-likelihood estimate of $\boldsymbol{m}$. Given the likelihood, we can use the Akaike information criterion [50, p. 209] for model selection,

$$\text{AIC} = -2\mathcal{L} + 2N_{\text{p}}. \quad (2.14)$$

We compare models via their difference in AIC, so the constant in equation (2.13*b*) cancels out.

2.3.5. Transmission rate reconstruction

In their study of the aggregate E&W measles times series, Fine & Clarkson [10] reconstructed the seasonally varying transmission rate $\beta(t)$ using a discrete-time SIR model. The meaning of this 'reconstruction' of $\beta(t)$ is that the 'reconstructed' $\beta(t)$ is the transmission rate that would yield the observed data if the underlying process were exactly a discrete-time SIR model in which the only source of time variation in parameter values is in the transmission rate. Thus, the 'reconstructed' $\beta(t)$ is really an *effective* transmission rate. The algorithm also 'reconstructs' (or perhaps more accurately *estimates*) the unobserved time series of susceptibles.

The discrete-time SIR model that Fine & Clarkson [10] used specifies the number of cases (C_t) and susceptibles (S_t) at times 0,1,2,..., where the time unit is a biweek (14 days), and the mean disease generation time T_{g} is also assumed to be a biweek (rather than the more precise 13 days). We follow Krylova [19], who found that a slight revision avoids the need to assume the reporting interval is equal to T_{g} (instead the reporting interval is taken to be a single week, as in reality, and T_{g} must simply be a multiple of the reporting interval). Assuming the time unit is the reporting interval (one week), the dynamic equations are

$$C_{t+T_{\text{g}}} = \beta_{t+T_{\text{g}}} S_{t+T_{\text{g}}} C_t \quad (2.15a)$$

and

$$S_{t+1} = S_t - \frac{1}{\eta} C_{t+1} + B_t - V_t - \mu S_t, \quad (2.15b)$$

where β_t, B_t and V_t denote the transmission rate and numbers of births and vaccinations, respectively, in time interval t, η is the proportion of cases reported and μ is the natural mortality rate. Given time series $\{\beta_t\}$, $\{B_t\}$ and $\{V_t\}$, and initial conditions (S_0, C_0), the discrete dynamic equations (2.15) can be iterated to produce discrete-time trajectories $\{(S_t, C_t)\}$ [31]. Fine & Clarkson [10] noted that for an observed time series of cases $\{C_t\}$, together with an estimated notification efficiency η and initial susceptible proportion S_0, equation (2.15) could instead be used to reconstruct the time series of susceptibles $\{S_t\}$ and transmission rate $\{\beta_t\}$. This can be achieved by solving equation (2.15*a*) for β_t, which yields [19, eqn (4.8)]

$$\beta_{t+T_{\text{g}}} = \frac{C_{t+T_{\text{g}}}}{S_{t+T_{\text{g}}} C_t}. \quad (2.16)$$

We used this method to reconstruct β_t from the E&W time series as well as from time series resulting from simulations of the various models we examined. When reconstructing β_t from a simulation, η and S_0 are known. To compare the reconstructed β_t from a model and from the E&W data, we fitted the model to the data (minimizing E_V as in §2.3.4) and then used the S_0 from the matched trajectory (electronic supplementary material, table S7) and the value of the notification efficiency that yields a piecewise horizontal β_t for the term-time SEIR model ($\eta = 0.71$).

The discretization in equation (2.15*a*) is over the mean generation time T_{g} (two weeks), which means that cases are integrated over a full generation time T_{g} and the reconstructed transmission rate β_t is *per generation time*. Consequently, because $\mathcal{R}_0 \sim \beta N/T_{\text{g}}$, we can interpret $\beta_t N$ as $\mathcal{R}_0$ and the time-averaged $\mathcal{R}_0$ can be estimated as $\langle \mathcal{R}_0 \rangle = \langle \beta_t \rangle N$.

2.4. Dynamic structure of the cohort-entry model

We used standard bifurcation and continuation software (XPPAUT) [51] to construct the bifurcation diagrams shown in figure 5*b*,*c*. Solid curves show attractors and dotted curves show repellers. A step-by-step guide to the procedure we used can be found in the electronic supplement to [8].

3. Results

3.1. Qualitative understanding of annual decline in transmission rate

Figure 3 shows the equivalent of figure 2 for the term-time forced SEIR model without age structure, but including the cohort effect as described in §2.2. Visual comparison of the top panels of these figures makes clear, qualitatively, that age structure is not necessary to capture the main features of the observed measles biennium. In addition, comparison of the bottom panels reveals that age structure is not required to capture the observed decline in the reconstructed effective transmission rate β_t over the course of each year.

Similar figures shown in the electronic supplementary material reinforce the inference that the cause of the annual decline in β_t is the cohort effect. Without the cohort effect, the effective β_t obtained by applying the reconstruction algorithm to solutions of the term-time SEIR model shows no decline (electronic supplementary material, figure S1), whereas without term-time forcing, the effective β_t reconstructed from solutions of the cohort-entry SEIR model shows decline but (unsurprisingly) no dips during school terms (electronic supplementary material, figure S2).

3.2. Quantitative fits of models to observed time series

Figure 4 compares the performance of the standard term-time forced SEIR model (figure 4*a*), the cohort-entry model without school-term forcing (figure 4*b*) and the full cohort and term-time forced model (figure 4*c*) in fitting the average E&W measles biennium. As detailed in Methods (§2), we follow previous work [42,43] and assess these deterministic models in terms of their ability to reproduce the average biennium for the period 1950–1964, and quantify the quality of the fits using the weighted fitting error E_V [42].

In each of the three panels of figure 4, the data are shown using a dashed black curve for the mean biennium ($X_{\text{obs}}(t)$, equation (2.6)) and grey shading extending to one standard deviation above and below the mean ($\pm\sqrt{V_{\text{obs}}(t)}$, equation (2.7)). For each model, the solid red curve shows the solution (after converging to the attractor) for the parameter set that minimizes E_V.

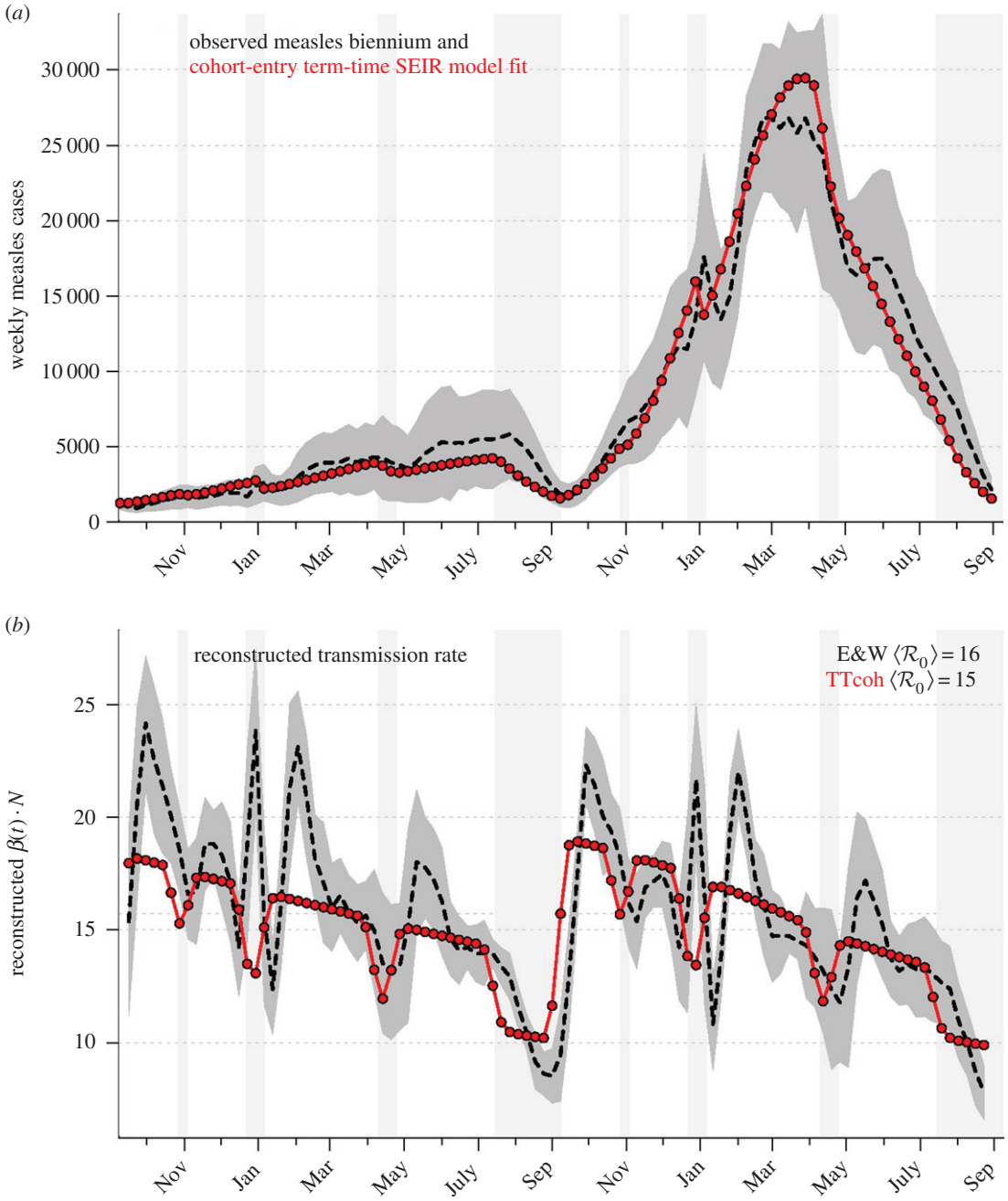

Figure 3. Equivalent of figure 2 for the cohort-entry SEIR model with term-time forcing. (Online version in colour.)

The inset graphs in each panel show profiles of E_V as a function of $\mathcal{R}_0$, i.e. for each $\mathcal{R}_0$, we find the values of all other free parameters that minimize E_V (black); thus, the minimum of the plotted E_V profile is the minimum in the full parameter space. The free parameters are the term-time forcing amplitude α, the cohort proportion c and the case *notification efficiency* η. The values of our focal parameters (α, c) that yield the minimum E_V for each $\mathcal{R}_0$ are also shown (term-time amplitude α in blue, cohort-entry proportion c in green).

Previous work fitting the term-time forced SEIR model to the same measles incidence time series [42,43] was conducted subject to the constraint that $\mathcal{R}_0 = 17$, the empirically estimated value [1, p. 70]. The resulting best fit with this constraint (reproducing fig. 5.15 of [43]) is shown as a dotted red curve in figure 4*a*. Allowing $\mathcal{R}_0$ to be fitted as well yields the solid red curve in figure 4*a*, but the fitted value ($\mathcal{R}_0 = 22.6$) is substantially higher than the empirical value. In contrast, without term-time forcing but with cohort-entry, figure 4*b* shows a fit that is just as good, with $\mathcal{R}_0 = 17$ arising from the fit rather than being specified in advance. Including both the school-term and cohort effects yields the best fit (lowest E_V), again yielding $\mathcal{R}_0 = 17$ without fixing $\mathcal{R}_0$ in advance. Note that while the cohort effect alone (figure 4*b*) succeeds in producing a formally good fit to the data, it fails to capture the small-scale temporal fluctuations arising from the three school terms, which are successfully reproduced in figure 4*c*. Table 1 summarizes the fits shown in figure 4, together with their associated ΔAIC values. The improvement obtained by including the cohort effect in addition to term-time forcing is highly significant.

In the electronic supplementary material, we repeat our analysis for several other measles incidence time series (see electronic supplementary material, figure S3) and obtain similar results (see electronic supplementary material, table S6). In addition, a much more elaborate and computationally demanding analysis of fully stochastic implementations of the models [25] also shows that significantly better fits of

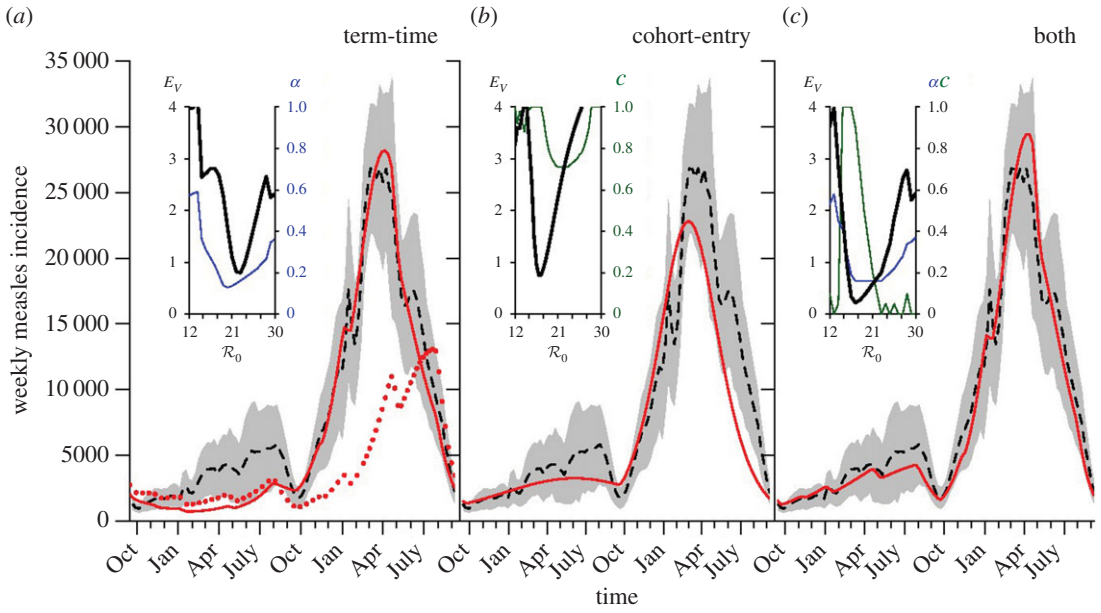

Figure 4. SEIR model fits (solid red) of the average measles biennium in England and Wales for the period 1950–1964 (dashed). Best fits were obtained as in previous work [40–43] by minimizing the weighted fitting error E_V (equation (2.9) and [42]). (*a*) The standard term-time forced SEIR model with forcing amplitude α (the dotted red curve shows the fit obtained by fixing $\mathcal{R}_0 = 17$ ([43] and fig. 5.15). (*b*) The cohort-entry model with cohort proportion c and no school-term forcing. (*c*) The full cohort and term-time forced model. In each panel, insets show profiles of E_V in black (and the associated minimizing values of α and c in blue and green, respectively) as a function of $\mathcal{R}_0$. Details are given in §3.2 and §2.3. The analysis is repeated for several city-level measles time series in electronic supplementary material, figure S4. (Online version in colour.)

Table 1. Parameter estimates obtained by fitting epidemic models to observed weekly measles cases in England and Wales, 1950–1964. Parameters that are not fitted are indicated with '—'.

model	c	α	$\mathcal{R}_0$	η	E_V	ΔAIC
term-time (fixed $\mathcal{R}_0 = 17$)	—	0.25	—	0.25	2.867	270.4
term-time	—	0.15	22.6	0.44	0.813	58.7
cohort-entry	1.00	—	17.2	0.43	0.732	50.3
both	1.00	0.16	17.1	0.49	0.229	0.0
RAS	—	—	13.4[a]	0.61	0.486	24.7

[a]For the RAS model, $\mathcal{R}_0$ was estimated as the mean of the reconstruction in figure 2. The fitted RAS parameters are described in electronic supplementary material, §2.3.

the detailed time series are achieved by including the cohort-entry effect (AIC_c is improved by more than 12 units).

3.3. Dynamic structure of the cohort-entry model

Predictions of structural changes in epidemic patterns, such as transitions between epidemic cycles of different lengths, depend primarily on qualitative analysis of models (e.g. bifurcation theory) rather than detailed quantitative fits of model-generated time series to case report time series. We therefore consider how the cohort effect influences predictions of bifurcations (e.g. transitions from annual to biennial or more complex dynamics).

Figure 5*a* shows the principal branches of the bifurcation tree (as a function of $\mathcal{R}_0$) of the term-time forced SEIR measles model ($c = 0$, $\alpha = 0.25$), which has been used previously [5,8,9,18,46] to predict the dynamic transitions evident in figure 1. Figure 5*b* shows the equivalent bifurcation tree for the cohort-entry SEIR model ($c = 0.8$, $\alpha = 0$). The topologies of the two bifurcation trees are identical and the positions ($\mathcal{R}_0$) of the bifurcations differ only slightly.[2] The striking similarity of the strict term-time forced ($c = 0$) and strict cohort-entry ($\alpha = 0$) models indicates that qualitative predictions of epidemic structure are very insensitive to the mechanistic origin of periodic seasonal forcing of the system.

Figure 5*c* summarizes the dynamics in the entire $\alpha - c$ plane for $\mathcal{R}_0 = 17$. The period-doubling bifurcation occurs on the curve marked 1 (red), whereas the other curves are contours of constant major-to-minor-peak-ratio for the biennial attractor (in London from 1950 to 1964 this ratio was approx. 5). Time series corresponding to the circled points on these curves are shown in the small numbered panels above figure 5*c*. A comparison of transient dynamics with and without cohort entry is presented in the electronic supplementary material, figure S6.

4. Discussion

In any situation where the rate of contact among children changes significantly when they first enter school, a cohort effect will influence the population dynamics of childhood infectious diseases. In our cohort-entry SEIR model, we

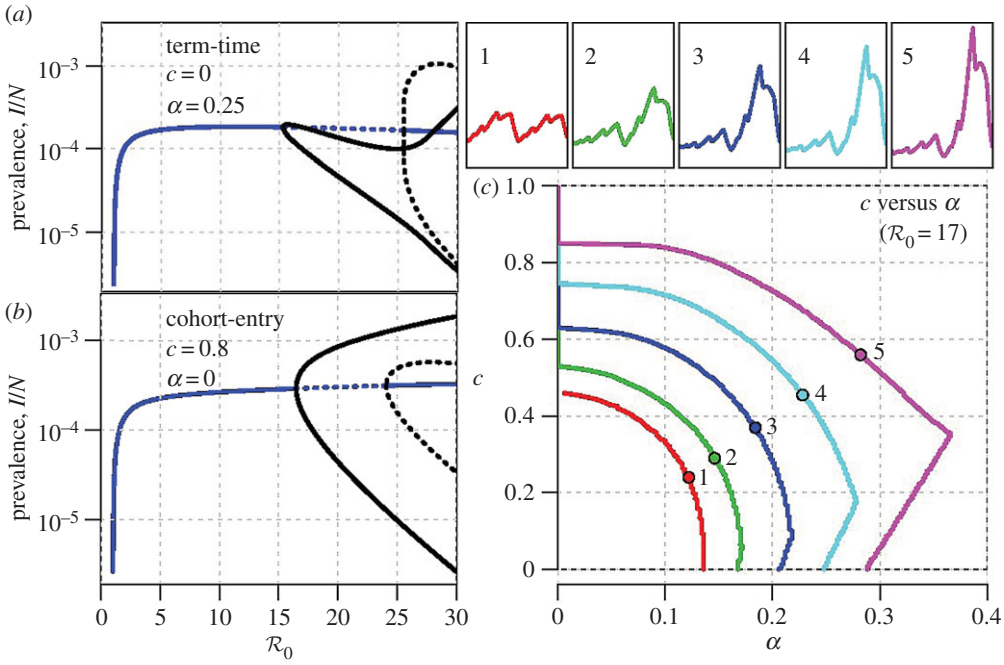

Figure 5. Dynamic structure of the term-time and cohort forced SEIR models. (*a*) The principal branches of the bifurcation tree (as a function of $\mathcal{R}_0$) of the term-time forced SEIR measles model ($c = 0$, $\alpha = 0.25$), which has been used previously [5,18,46] to predict the dynamic transitions evident in figure 1. (*b*) The equivalent bifurcation tree for the cohort-entry model ($c = 0.8$, $\alpha = 0$). (*c*) Dynamics in the entire α–c plane for $\mathcal{R}_0 = 17$. The period-doubling bifurcation occurs on the curve marked 1 (red), whereas the other curves are contours of constant major-to-minor-peak-ratio for the biennial attractor (the ratio is marked on each curve; in London, 1950–1964, this ratio was approx. 5). Time series corresponding to the circled points on these curves are shown in the small numbered panels above panel (*c*). The equivalents of panel (*c*) for other values of $\mathcal{R}_0$ are shown in the electronic supplementary material, figure S5. (Online version in colour.)

formalized this effect using an annual pulse in the birth term; a proportion c of children begins contacting others on the day schools open, whereas the remainder enter the well-mixed population when they are born (equation (2.4)). We have considered the cohort effect in general and in the specific context of measles, a well-studied childhood disease for which lengthy high-quality notification time series exist for a variety of locations.

Complex observed patterns of measles incidence have captured the attention of mathematical ecologists and epidemiologists since the seminal work of Bartlett [52–54] in the 1950s. In an attempt to understand measles dynamics, Schenzle [37] developed a realistic age-structured (RAS) model using a system of 84 differential equations that specify the time variation of the numbers of susceptible (S), exposed (E), infectious (I) and recovered (R) individuals in each of 21 age classes (see electronic supplementary material, §2). The model includes term-time forcing of contacts among school-age children, and entry of a new cohort and gradewise movement at the start of each school year. The RAS model provides a good fit to the averaged biennial cycle of measles epidemics observed in E&W in the pre-vaccine era (1948–1968) [37] and with the fitted parameters does not predict chaotic dynamics [40], in contrast to the simpler sinusoidally forced SEIR model [4].

The global dynamics of the RAS model are, in fact, primarily driven by term-time forcing of the transmission rate, rather than age structure [5]. This realization has made it possible to explain changes in outbreak frequency in many infectious disease time series, using the term-time forced SEIR model or other simple epidemic models [5,8,9,17–19,46].

One aspect of real measles dynamics that is captured by the RAS model but not the simpler term-time forced SEIR model is the decline in the effective (reconstructed) transmission rate $\beta(t)$ over the course of the school year (figure 2). In this paper, we have shown that the decline in the reconstructed $\beta(t)$ arises from the cohort effect, not from age structure *per se* (figure 3).

The cohort-entry SEIR model that we have examined here is essentially equivalent to the two-age-class limit of the RAS model in which there is no transmission in the younger age class. Andreasen & Frommelt [55] presented a different cohort-entry-age-structured model, which has the virtue of being amenable to some useful analytical investigation (unlike the RAS model and the simpler SEIR models considered here). The effects of birth pulses on epidemics in animal populations have been studied previously [49].

Previous work has shown that matching trajectories of the term-time forced SEIR model to the average measles biennium in E&W yields an unrealistically high estimate of the basic reproduction number $\mathcal{R}_0$ [42,43]. We compared the fits obtained using the term-time forced SEIR model (figure 4*a*) with fits obtained using SEIR models incorporating the cohort-entry effect, both with and without seasonality in the transmission rate (figure 4*b*,*c*). We obtained significantly better fits, with an estimated $\mathcal{R}_0$ closer to the conventional value [1, p. 70], by including the cohort-entry effect. Moreover, when we include both cohort-entry and transmission rate seasonality, the fit to the E&W measles biennium is just as good as that obtained with the RAS model.

We studied the global dynamic structure of the cohort-entry SEIR model and found that the bifurcation tree is topologically equivalent, regardless of whether transmission rate seasonality is included (figure 5). Thus, from the point of view of qualitative dynamics, the source of seasonal forcing may be irrelevant in the SEIR model.

Age-structured models are important and natural tools to use in the development of control strategies for childhood diseases [56], because optimal control strategies are

themselves likely to be age-structured. However, when using models that include many biological details, the roles of individual biological mechanisms may be obscured. Our formalization of the cohort-entry SEIR model without explicit age structure has allowed us to reveal that the cohort effect alone is sufficient to generate an annual decline in the effective (reconstructed) transmission rate, as is often observed (cf. figures 2*b* and 3*b*; and electronic supplementary material, figures S1 and S2). In addition, our analyses of particular measles time series indicated that the best-fit cohort proportion is large (electronic supplementary material, table S6), suggesting that most children younger than school age are also indirectly subject to the cohort effect, presumably because they interact with older siblings and other schoolchildren.

Data accessibility. All the data studied in this paper are available either from the electronic supplementary material or from the International Infectious Disease Data Archive (IIDDA) at http://iidda.mcmaster.ca.

Authors' contributions. Both authors conceived and carried out the study, drafted the manuscript and gave final approval for publication.

Competing interests. We have no competing interests.

Funding. D.E. was supported by grants from NSERC, CIHR and the J. S. McDonnell Foundation. D.H. was supported by an Early Career Scheme grant from the Hong Kong Research Grant Council (25100114), and a Health and Medical Research Grant from the Hong Kong Food and Health Bureau Research Council (13121382).

Acknowledgements. We are grateful to Ben Bolker for valuable comments.

Endnotes

[1]'In England term starts in September, [and in] the entry year children must be 5 before August 31 the following year.' (http://resources.woodlands-junior.kent.sch.uk/customs/questions/education/startsch.html).

[2]We show only the principal branch of the bifurcation trees in figure 5*a*. The positions of bifurcations on other branches (corresponding to longer period cycles) do differ more substantially among models, but these branches have no detectable effect on the dynamics [18,46] and do not exist in the presence of a small amount of infective immigration (e.g. proportion 10^{-7} of total population size per year).

References

1. Anderson RM, May RM. 1991 *Infectious diseases of humans: dynamics and control*. Oxford, UK: Oxford University Press.
2. Hethcote HW. 2000 The mathematics of infectious diseases. *SIAM Rev.* **42**, 599–653. (doi:10.1137/S0036144500371907)
3. London W, Yorke JA. 1973 Recurrent outbreaks of measles, chickenpox and mumps. I. Seasonal variation in contact rates. *Am. J. Epidemiol.* **98**, 453–468.
4. Olsen LF, Schaffer WM. 1990 Chaos versus noisy periodicity: alternative hypotheses for childhood epidemics. *Science* **249**, 499–504. (doi:10.1126/science.2382131)
5. Earn DJD, Rohani P, Bolker BM, Grenfell BT. 2000 A simple model for complex dynamical transitions in epidemics. *Science* **287**, 667–670. (doi:10.1126/science.287.5453.667)
6. Ferrari MJ, Grais RF, Bharti N, Conlan AJK, Bjornstad ON, Wolfson LJ, Guerin PJ, Djibo A, Grenfell BT. 2008 The dynamics of measles in sub-Saharan Africa. *Nature* **451**, 679–684. (doi:10.1038/nature06509)
7. Hooker G, Ellner SP, De Vargas Roditi L, Earn DJD. 2011 Parameterizing state-space models for infectious disease dynamics by generalized profiling: measles in Ontario. *J. R. Soc. Interface* **8**, 961–974. (doi:10.1098/rsif.2010.0412)
8. Krylova O, Earn DJD. 2013 Effects of the infectious period distribution on predicted transitions in childhood disease dynamics. *J. R. Soc. Interface* **10**, 20130098. (doi:10.1098/rsif.2013.0098)
9. Hempel K, Earn DJD. 2015 A century of transitions in New York City's measles dynamics. *J. R. Soc. Interface* **12**, 20150024. (doi:10.1098/rsif.2015.0024)
10. Fine PEM, Clarkson JA. 1982 Measles in England and Wales I: an analysis of factors underlying seasonal patterns. *Int. J. Epidemiol.* **11**, 5–14. (doi:10.1093/ije/11.1.5)
11. Fine PEM, Clarkson JA. 1982 Measles in England and Wales II: the impact of the measles vaccination programme on the distribution of immunity in population. *Int. J. Epidemiol.* **11**, 15–25. (doi:10.1093/ije/11.1.15)
12. He D, Earn DJD. 2007 Epidemiological effects of seasonal oscillations in birth rates. *Theor. Popul. Biol.* **72**, 274–291. (doi:10.1016/j.tpb.2007.04.004)
13. Shaman J, Pitzer VE, Viboud C, Grenfell BT, Lipsitch M. 2010 Absolute humidity and the seasonal onset of influenza in the continental United States. *PLoS Biol.* **8**, e1000316. (doi:10.1371/journal.pbio.1000316)
14. Earn DJD, He D, Loeb MB, Fonseca K, Lee BE, Dushoff J. 2012 Effects of school closure on incidence of pandemic influenza in Alberta, Canada. *Ann. Intern. Med.* **156**, 173–181. (doi:10.7326/0003-4819-156-3-201202070-00005)
15. Lima M. 2009 A link between the north Atlantic oscillation and measles dynamics during the vaccination period in England and Wales. *Ecol. Lett.* **12**, 302–314. (doi:10.1111/j.1461-0248.2009.01289.x).
16. Brauer F, Castillo-Chavez C. 2001 *Mathematical models in population biology and epidemiology*. Texts in Applied Mathematics, vol. 40. New York, NY: Springer. (doi:10.1007/978-1-4614-1686-9)
17. Bauch CT, Earn DJD. 2003 Interepidemic intervals in forced and unforced SEIR models. In *Dynamical systems and their applications in biology* (eds S Ruan, G Wolkowicz, J Wu), vol. 36 of *Fields Institute Communications*, pp. 33–44. Toronto, Canada: American Mathematical Society.
18. Earn DJD. 2009 Mathematical epidemiology of infectious diseases. In *Mathematical biology* (eds MA Lewis, MAJ Chaplain, JP Keener, PK Maini), vol. 14 of *IAS/Park City Mathematics Series*, pp. 151–186. American Mathematical Society.
19. Krylova O. 2011 Predicting epidemiological transitions in infectious disease dynamics: smallpox in historic London (1664–1930). PhD thesis, McMaster University, Hamilton, Ontario, Canada.
20. Pollicott M, Wang H, Weiss H. 2012 Extracting the time-dependent transmission rate from infection data via solution of an inverse ode problem. *J. Biol. Dyn.* **6**, 509–523. (doi:10.1080/17513758.2011.645510)
21. Lange A. 2016 Reconstruction of disease transmission rates: applications to measles, dengue, and influenza. *J. Theor. Biol.* **400**, 138–153. (doi:10.1016/j.jtbi.2016.04.017)
22. deJonge MS. 2014 Fast estimation of time-varying transmission rates for infectious diseases. MSc thesis, McMaster University, Hamilton, Ontario, Canada.
23. Finkenstädt B, Grenfell B. 2000 Time series modelling of childhood diseases: a dynamical systems approach. *J. R. Stat. Soc. C* **49**, 187–205. (doi:10.1111/1467-9876.00187)
24. Breto C, He DH, Ionides EL, King AA. 2009 Time series analysis via mechanistic models. *Ann. Appl. Stat.* **3**, 319–348. (doi:10.1214/08-AOAS201)
25. He D, Ionides EL, King AA. 2010 Plug-and-play inference for disease dynamics: measles in large and small populations as a case study. *J. R. Soc. Interface* **7**, 271–283. (doi:10.1098/rsif.2009.0151)
26. Ramsay JO, Hooker G, Campbell D, Cao J. 2007 Parameter estimation for differential equations: a generalized smoothing approach. *J. R. Stat. Soc. B* **69**, 741–796. (doi:10.1111/j.1467-9868.2007.00610.x)
27. Cao J, Fussmann GF, Ramsay JO. 2008 Estimating a predator-prey dynamical model with the parameter cascades method. *Biometrics* **64**, 959–967. (doi:10.1111/j.1541-0420.2007.00942.x)
28. Wallinga J, Teunis P. 2004 Different epidemic curves for severe acute respiratory syndrome reveal similar

impacts of control measures. *Am. J. Epidemiol.* **160**, 509–516. (doi:10.1093/aje/kwh255)

29. Goldstein E, Dushoff J, Ma J, Plotkin J, Earn DJD, Lipsitch M. 2009 Reconstructing influenza incidence by deconvolution of daily mortality time series. *Proc. Natl Acad. Sci. USA* **106**, 21 825–21 829. (doi:10.1073/pnas.0902958106)
30. Fine PE, Clarkson JA. 1983 Measles in England and Wales—III: assessing published predictions of the impact of vaccination of incidence. *Int. J. Epidemiol.* **12**, 332–339. (doi:10.1093/ije/12.3.332)
31. Mollison D, Din SU. 1993 Deterministic and stochastic models for the seasonal variability of measles transmission. *Math. Biosci.* **117**, 155–177. (doi:10.1016/0025-5564(93)90021-2)
32. Black AJ, McKane AJ. 2010 Stochasticity in staged models of epidemics: quantifying the dynamics of whooping cough. *J. R. Soc. Interface* **7**, 1219–1227. (doi:10.1098/rsif.2009.0514)
33. Clarkson JA, Fine PEM. 1985 The efficiency of measles and pertussis notification in England and Wales. *Int. J. Epidemiol.* **14**, 153–168. (doi:10.1093/ije/14.1.153)
34. Rohani P, Earn DJD, Finkenstadt B, Grenfell BT. 1998 Population dynamic interference among childhood diseases. *Proc. R. Soc. Lond. B* **265**, 2033–2041. (doi:10.1098/rspb.1998.0537)
35. Finkenstädt BF, Grenfell BT. 1998 Empirical determinants of measles metapopulation dynamics in England and Wales. *Proc. R. Soc. Lond. B* **265**, 211–220. (doi:10.1098/rspb.1998.0284)
36. Rohani P, Keeling MJ, Grenfell BT. 2002 The interplay between determinism and stochasticity in childhood diseases. *Am. Nat.* **159**, 469–481. (doi:10.1086/339467)
37. Schenzle D. 1984 An age-structured model of pre- and post-vaccination measles transmission. *IMA J. Math. Appl. Med. Biol.* **1**, 169–191. (doi:10.1093/imammb/1.2.169)
38. Ellner SP, Bailey BA, Bobashev GV, Gallant AR, Grenfell BT, Nychka DW. 1998 Noise and nonlinearity in measles epidemics: combining mechanistic and statistical approaches to population modeling. *Am. Nat.* **151**, 425–440. (doi:10.1086/286130)
39. Bolker B. 1993 Chaos and complexity in measles models: a comparative numerical study. *IMA J. Math. Appl. Med. Biol.* **10**, 83–95. (doi:10.1093/imammb/10.2.83)
40. Bolker BM, Grenfell BT. 1993 Chaos and biological complexity in measles dynamics. *Proc. R. Soc. Lond. B* **251**, 75–81. (doi:10.1098/rspb.1993.0011)
41. Babad HR, Nokes DJ, Gay NJ, Miller E, Morgancapner P, Anderson RM. 1995 Predicting the impact of measles vaccination in England and Wales: model validation and analysis of policy options. *Epidemiol. Infect.* **114**, 319–344. (doi:10.1017/S0950268800057976)
42. Keeling MJ, Grenfell BT. 2002 Understanding the persistence of measles: reconciling theory, simulation and observation. *Proc. R. Soc. Lond. B* **269**, 335–343. (doi:10.1098/rspb.2001.1898)
43. Keeling MJ, Rohani P. 2008 *Modeling infectious diseases in humans and animals*. Princeton, NJ: Princeton University Press.
44. Education Act. 1944 London, UK: HMSO. See http://www.educationengland.org.uk/documents/acts/1944-education-act.pdf.
45. He D. 2006 Modeling of childhood infectious diseases. PhD thesis, McMaster University, Hamilton, Ontario, Canada.
46. Bauch CT, Earn DJD. 2003 Transients and attractors in epidemics. *Proc. R. Soc. Lond. B* **270**, 1573–1578. (doi:10.1098/rspb.2003.2410)
47. Ma J, Ma Z. 2006 Epidemic threshold conditions for seasonally forced SEIR models. *Math. Biosci. Eng.* **3**, 161–172. (doi:10.3934/mbe.2006.3.161)
48. Shulgin B, Stone L, Agur Z. 1998 Pulse vaccination strategy in the SIR epidemic model. *Bull. Math. Biol.* **60**, 1123–1148. (doi:10.1016/S0092-8240(98)90005-2)
49. Roberts MG, Kao RR. 1998 The dynamics of an infectious disease in a population with birth pulses. *Math. Biosci.* **149**, 23–36. (doi:10.1016/S0025-5564(97)10016-5)
50. Bolker BM. 2008 *Ecological models and data in R*. Princeton, NJ: Princeton University Press.
51. Ermentrout B. 2002 *Simulating, analyzing, and animating dynamical systems: a guide to XPPAUT for researchers and students*. Software, environments, and tools. Philadelphia, PA: Society for Industrial and Applied Mathematics.
52. Bartlett MS. 1957 Measles periodicity and community size. *J. R. Stat. Soc. A* **120**, 48–70. (doi:10.2307/2342553)
53. Bartlett MS. 1960 *Stochastic population models in ecology and epidemiology, volume 4 of Methuen's monographs on applied probability and statistics*. London, UK: Spottiswoode, Ballantyne & Co. Ltd.
54. Bartlett MS. 1961 Monte Carlo studies in ecology and epidemiology. In *4th Berkeley Symp. on Mathematical Statistics and Probability* (ed. J Neyman), vol. 4: *contributions to biology and problems of medicine*, pp. 39–55. Statistical Laboratory of the University of California, Berkeley, CA: University of California Press.
55. Andreasen V, Frommelt T. 2005 A school-oriented, age-structured epidemic model. *SIAM J. Appl. Math.* **65**, 1870–1887. (doi:10.1137/040610684)
56. Ramsay M, Gay N, Miller E, Rush M, White J, Morgan-Capner P, Brown D. 1994 The epidemiology of measles in England and Wales: rationale for the 1994 national vaccination campaign. *Commun. Dis. Rep. CDR Rev.* **4**, R141–R146.

The cohort effect in childhood disease dynamics
ELECTRONIC SUPPLEMENTARY MATERIAL

Daihai He[1,2] **and David J.D. Earn**[2]

[1]Department of Applied Mathematics,
Hong Kong Polytechnic University, Hung Hom, Kowloon, Hong Kong;

[2]Department of Mathematics and Statistics,
McMaster University, Hamilton, Ontario, Canada, L8S 4K1

June 18, 2016 @ 13:09

Contents

1 Data

All the data studied in this paper are available either from the journal website as Electronic Supplementary Material or from the International Infectious Disease Data Archive (IIDDA) at

http://IIDDA.McMaster.ca.

The specific data files are listed below.

1.1 Measles incidence

Measles incidence in the UK were published in the Registrar General's Weekly Returns for England and Wales. Monthly measles notifications in New York City, 1928–1973, were tabulated by London and Yorke [1, 2] (a longer measles time series for NYC was recently digitized and made available by Hempel and Earn [3]).

- Weekly reported measles in England and Wales, 1948–1966:
  meas_uk_ew_1948-66_wk.csv.
- Weekly reported measles in London, England, 1944–1994:
  meas_uk_london_1944-94_wk.csv
- Weekly reported measles in Liverpool, England, 1944–1994:
  meas_uk_liverpool_1944-94_wk.csv
- Monthly reported measles in New York City, USA, 1928–1963:
  meas_us_nyc_1928-63_mn.csv

1.2 Annual population sizes and birth rates

Published annual population size and numbers of live births in England and Wales were obtained from "Population estimates for England and Wales by total persons, males and females – Mid-1838 to Mid-2013" and "Live birth 1938–2013", UK Office for National Statistics (http://www.ons.gov.uk).

- Yearly births in London, UK, 1944–1994:
  bth_uk_lon_1944-94_yr.csv
- Yearly births in Liverpool, UK, 1944–1994:
  bth_uk_lpl_1944-94_yr.csv
- Yearly Birth rate in New York City, USA, 1925–1963:
  bthrt_us_ny_1925-63_yr.csv

1.3 Average population sizes and birth rates

Table S1 gives the average population sizes and average birth rates for the four locations studied in this paper. The source for E&W as a whole and the cities of London and Liverpool is

http://www.visionofbritain.org.uk/.

The source for New York City is the NYC Department of Health's *Summary of Vital Statistics* for 1961 for the city of New York, which can be obtained from:

http://www.nyc.gov/html/doh/downloads/pdf/vs/1961sum.pdf.

Table S1: Population sizes and birth rates during the periods of biennial cycles of measles epidemics examined in this paper.

Place	Population	Birth rate
E&W (UK)	45,000,000	0.02 / yr
London (UK)	3,300,000	0.017 / yr
Liverpool (UK)	760,000	0.021 / yr
NYC (US)	7,800,000	0.021 / yr

2 Realistic Age-Structured (RAS) model

Schenzle's [4] realistic age structured (RAS) model contains 21 age classes, each of which is subdivided into four compartments: susceptible (S_i), exposed (E_i), infectious (I_i), and recovered (R_i), for $i = 0, 1, \ldots, 20$. The population size in each age class is $N_i = S_i + E_i + I_i + R_i$. Births occur into the lowest age class continuously. The simple transmission rate $\beta(t)$ of the SEIR model (**equation** (1)) is replaced by a transmission matrix $\beta_{ij}(t)$, which includes term-time forcing in primary school (ages 6–10). Initial school entry and grade-wise movement of cohorts occur on the first day of school each year.

2.1 RAS model equations

For convenience, we write the force of infection in age class i as

$$\lambda_i = \sum_{j=0}^{20} \beta_{ij} I_j \,, \tag{S1}$$

where β_{ij} is given in **Table S4**. Following Schenzle [4], we assume that deaths occur only in the oldest age class (20+). Newborns enter S_0. Thus, for age-class-0

$$\dot{S}_0 = \nu N_{20} - \lambda_0 S_0 \tag{S2a}$$
$$\dot{E}_0 = \lambda_0 S_0 - \sigma E_0 \tag{S2b}$$
$$\dot{I}_0 = \sigma E_0 - \gamma I_0 \tag{S2c}$$
$$\dot{R}_0 = \gamma I_0 \tag{S2d}$$

For age-class-1 to age-class-19

$$\begin{aligned} \dot{S}_i &= -\lambda_i S_i && \text{(S3a)} \\ \dot{E}_i &= \lambda_i S_i - \sigma E_i && \text{(S3b)} \\ \dot{I}_i &= \sigma E_i - \gamma I_i && \text{(S3c)} \\ \dot{R}_i &= \gamma I_i && \text{(S3d)} \end{aligned}$$

Finally, in age-class-20+ there are deaths as well:

$$\begin{aligned} \dot{S_{20}} &= -\lambda_{20} S_{20} - \mu S_{20} && \text{(S4a)} \\ \dot{E_{20}} &= \lambda_{20} S_{20} - \sigma E_{20} - \mu E_{20} && \text{(S4b)} \\ \dot{I_{20}} &= \sigma E_{20} - \gamma I_{20} - \mu I_{20} && \text{(S4c)} \\ \dot{R_{20}} &= \gamma I_{20} - \mu R_{20} && \text{(S4d)} \end{aligned}$$

On the first day of school each year, we have

$$\begin{aligned} S_0 &= 0 && \text{(S5a)} \\ E_0 &= 0 && \text{(S5b)} \\ I_0 &= 0 && \text{(S5c)} \\ R_0 &= 0 && \text{(S5d)} \end{aligned}$$

and for $i = 1, \ldots, 19$,

$$\begin{aligned} S_i &= S_{i-1} && \text{(S6a)} \\ E_i &= E_{i-1} && \text{(S6b)} \\ I_i &= I_{i-1} && \text{(S6c)} \\ R_i &= R_{i-1} && \text{(S6d)} \end{aligned}$$

Finally,

$$\begin{aligned} S_{20} &= S_{20} + S_{19} && \text{(S7a)} \\ E_{20} &= E_{20} + E_{19} && \text{(S7b)} \\ I_{20} &= I_{20} + I_{19} && \text{(S7c)} \\ R_{20} &= R_{20} + R_{19} && \text{(S7d)} \end{aligned}$$

2.2 Initial conditions

The initial proportions of the population in each age class are given in **Table S2**. This initial age distribution is based on the published age structure of the UK in 1971:

> http://www.ons.gov.uk/ons/interactive/uk-population-pyramid---dvc1/index.html

This initial setting turns out to be irrelevant, since Schenzle's [4] model approaches a different equilibrium age structure: All age classes (except for 20+) converge to an equilibrium population size x, where $x = \nu(N - 20x)$ and hence [5]

$$x = \frac{N}{20 + 1/\nu} = 642857\,. \qquad \text{(S8)}$$

The initial conditions for the state variables are

$$S_i = 0.001N\,, \tag{S9a}$$
$$E_i = I_i = 0.000001N\,, \tag{S9b}$$
$$R_i = N_i - S_i - E_i - I_i\,, \tag{S9c}$$

where N_i is the initial proportion of the population in age-class i (**Table S2**).

Table S2: Initial proportions of the population in each age class.

Age Classes	Symbols	Percentage
0–4	$N_0, \ldots, N_3$	1.6
4–9	$N_4, \ldots, N_8$	1.7
9–11	N_9, N_{10}	1.6
11–13	N_{11}, N_{12}	1.5
13–20	$N_{13}, \ldots, N_{19}$	1.4
21+	N_{20}	69

2.3 Parameter values

Several fixed parameter values are listed in **Table S3**.

Table S3: Fixed parameters for the RAS model.

Parameter	Symbol	Value
Population size	N	45 million
Birth rate	ν	$0.02\,\mathrm{yr}^{-1}$
Death rate	μ	$0.02\,\mathrm{yr}^{-1}$
Mean latent period	σ^{-1}	8 days
Mean infectious period	γ^{-1}	5 days

Since the number of parameters in the RAS model is large (441 matrix entries β_{ij}), simplifying assumptions are typically made to reduce the number of free parameters. We follow previous work ([4], [6], [7, p. 85]) and assume that β_{ij} is a symmetric matrix with identical entries for sequences of age classes (**Table S4**, multiplied by an overall factor b_0). The function $b(t)$ in the second diagonal entry of **Table S4** is

$$b(t) = \begin{cases} b_2 & \text{during school terms,} \\ 0 & \text{otherwise.} \end{cases} \tag{S10}$$

Our best-fit parameter values are given in **Table S5**. Note that the best-fit RAS model yields $E_V = 0.486$, whereas the best-fit term-time cohort-entry model yields $E_V = 0.229$.

Table S4: Transmission matrix structure for the RAS model. Each entry is actually multiplied by the factor b_0 given in **Table S5**.

	age 0–5	age 6–9	age 10–19	age 20+
age 0–5	2.175	2.175	0.975	0.6
age 6–9	2.175	$2.175 + b(t)$	0.975	0.6
age 10–19	0.975	0.975	0.975	0.6
age 20+	0.6	0.6	0.6	0.6

Table S5: Fitted parameters for the RAS model.

Parameter	Symbol	Value
Overall transmission factor	b_0	398.6
School transmission enhancement	b_2	18.23
Reporting ratio	η	0.61

3 Alternative formulation of cohort entry model

The total population size, $N = S + E + I + R$, does not appear explicitly in **equation** (1). If the population size is constant (so $B = \mu N$) then it has no dynamical effect. If $B = \nu N$ (where ν is the *per capita* birth rate) and $\beta = \beta'/N$ (where β' is constant) then the equations for the proportions of individuals in each compartment (S/N, E/N, *etc.*) do not contain N so, again, population size has no dynamical effect [8]. If B is constant but $B \neq \mu N$ then population size *does* affect the dynamics. Which formulation is appropriate depends on the biological context and the questions that are being addressed. For childhood infectious diseases in modern cities, **equation** (1) with constant B ($B \neq \mu N$) is the most successful in terms of predicting qualitative dynamical changes in observed incidence time series [9–11].

Note that if we re-express the SEIR model in terms of proportions of the population in each compartment then B appears instead of μ in the mortality terms of **equation** (1) [8], in which case there are several places where we need to substitute $B \to \widetilde{B}(t)$. He [12] investigated this alternative formulation of the cohort entry model and found results that are qualitatively identical and quantitatively nearly identical as those presented in this paper. In particular, the topology of the bifurcation tree (**Figure 5**(c)) is identical and the positions ($\mathcal{R}_0$) of the bifurcations differ only slightly. See **Figure S5**(a).

As mentioned in the introduction, the cohort-entry model is similar to a two-age-class limit of the RAS model. He [12, Figure 3.19, p. 101] compared the cohort-entry model with a two-age-class model and found that they had similar, but not identical, dynamics.

4 Transmission rate reconstruction

Figure S1 and **Figure S2** show the equivalents of **Figure 2** and **Figure 3** for the SEIR model with term-time forcing but without the cohort effect (**Figure S1**) and with the cohort effect but without any seasonal forcing (**Figure S2**).

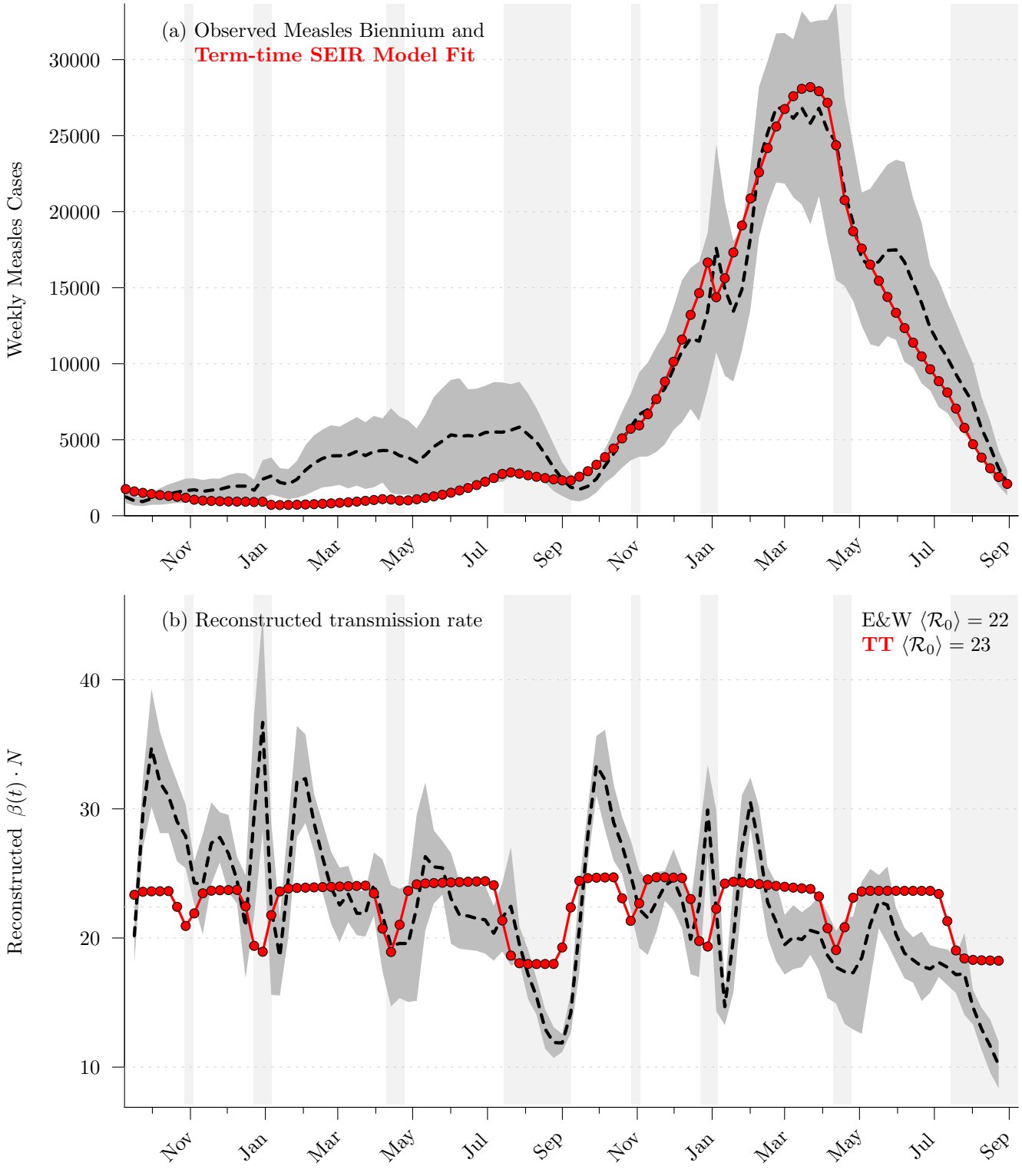

Figure S1: Equivalent of **Figure 2** for the SEIR model with term-time forcing.

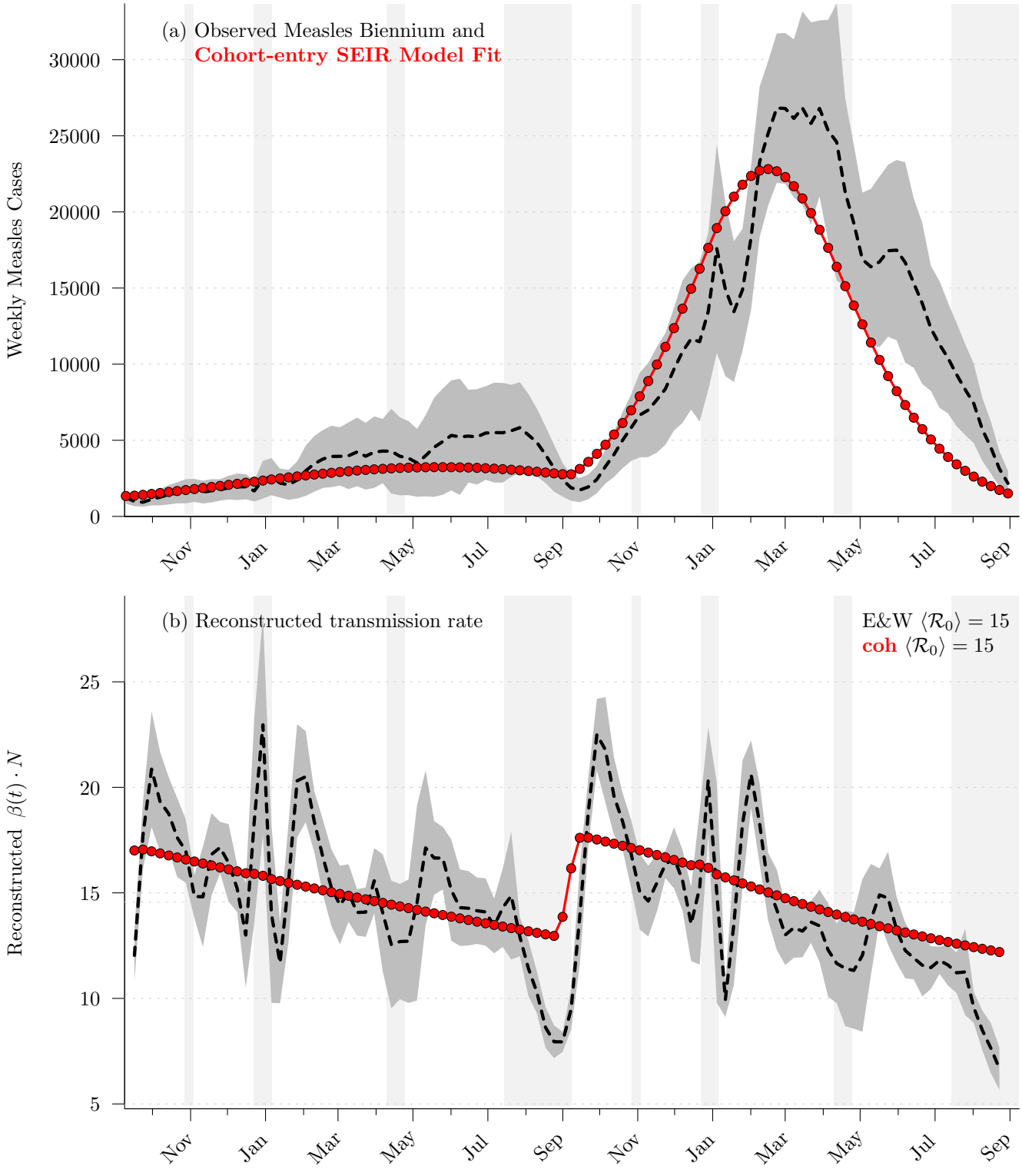

Figure S2: Equivalent of **Figure 2** for the cohort entry SEIR model.

5 City-level measles and demographic data

Figure 1 shows the aggregate E&W weekly measles data studied by Fine and Clarkson [13], together with annual rates of birth and susceptible recruitment. **Figure S3**(a) shows the E&W aggregate data again, while **Figure S3**(b–d) show the corresponding data for three individual cities (London and Liverpool in the the UK and New York City).

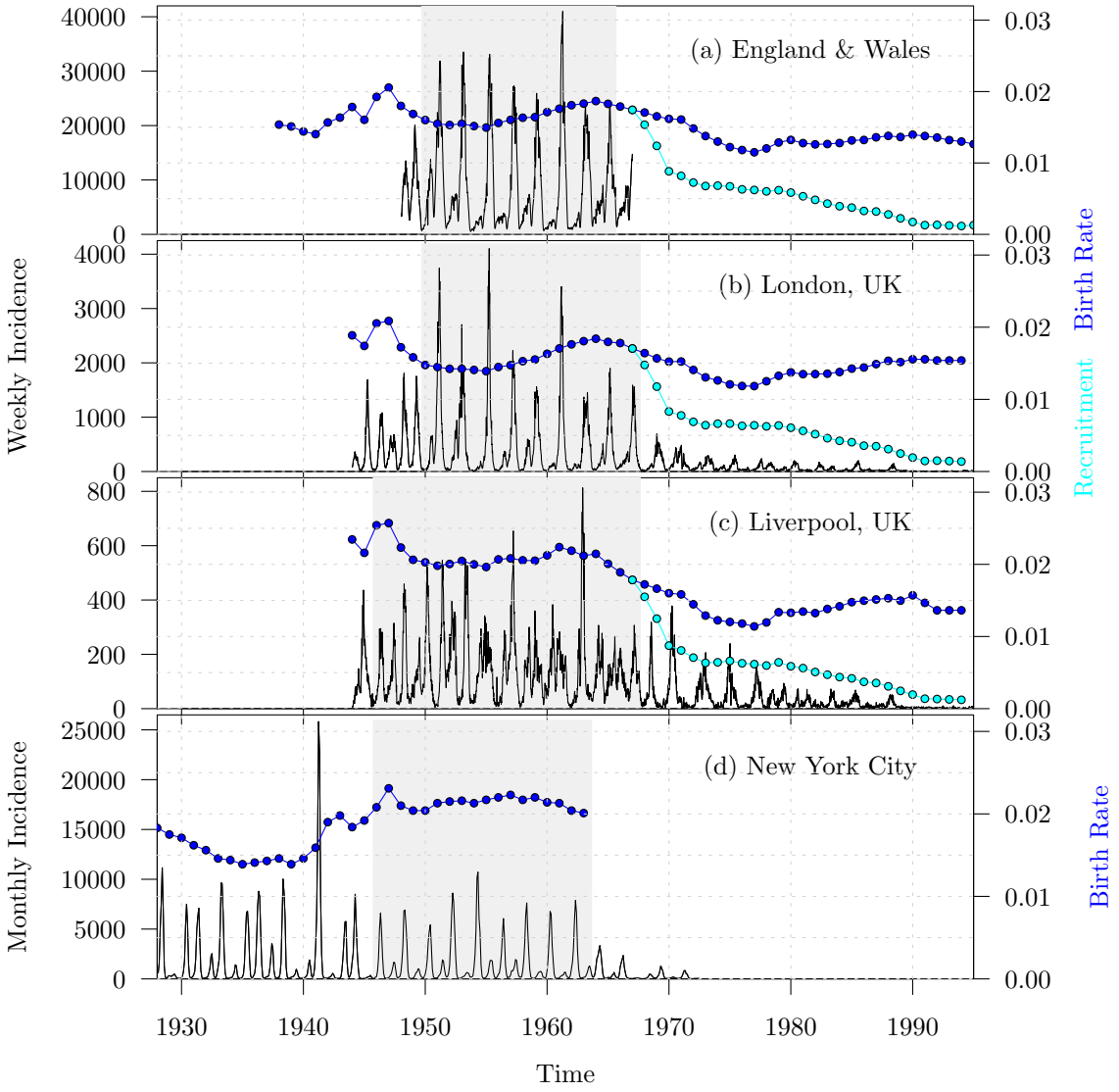

Figure S3: Measles incidence and concurrent demographic data in England and Wales and three individual cities. The four panels show measles incidence (black solid curve, weekly for the UK and monthly for the US), annual birth rate (blue) and susceptible recruitment (cyan) in England & Wales, London (UK), Liverpool (UK) and New York City (US), respectively. In each panel, the time interval that we used to compare with the biennial attractor of various models is highlighted with grey shading.

6 City-level measles biennium fits

Figure S4 shows the equivalent of **Figure 4** for the three city-level measles time series shown in **Figure S3**.

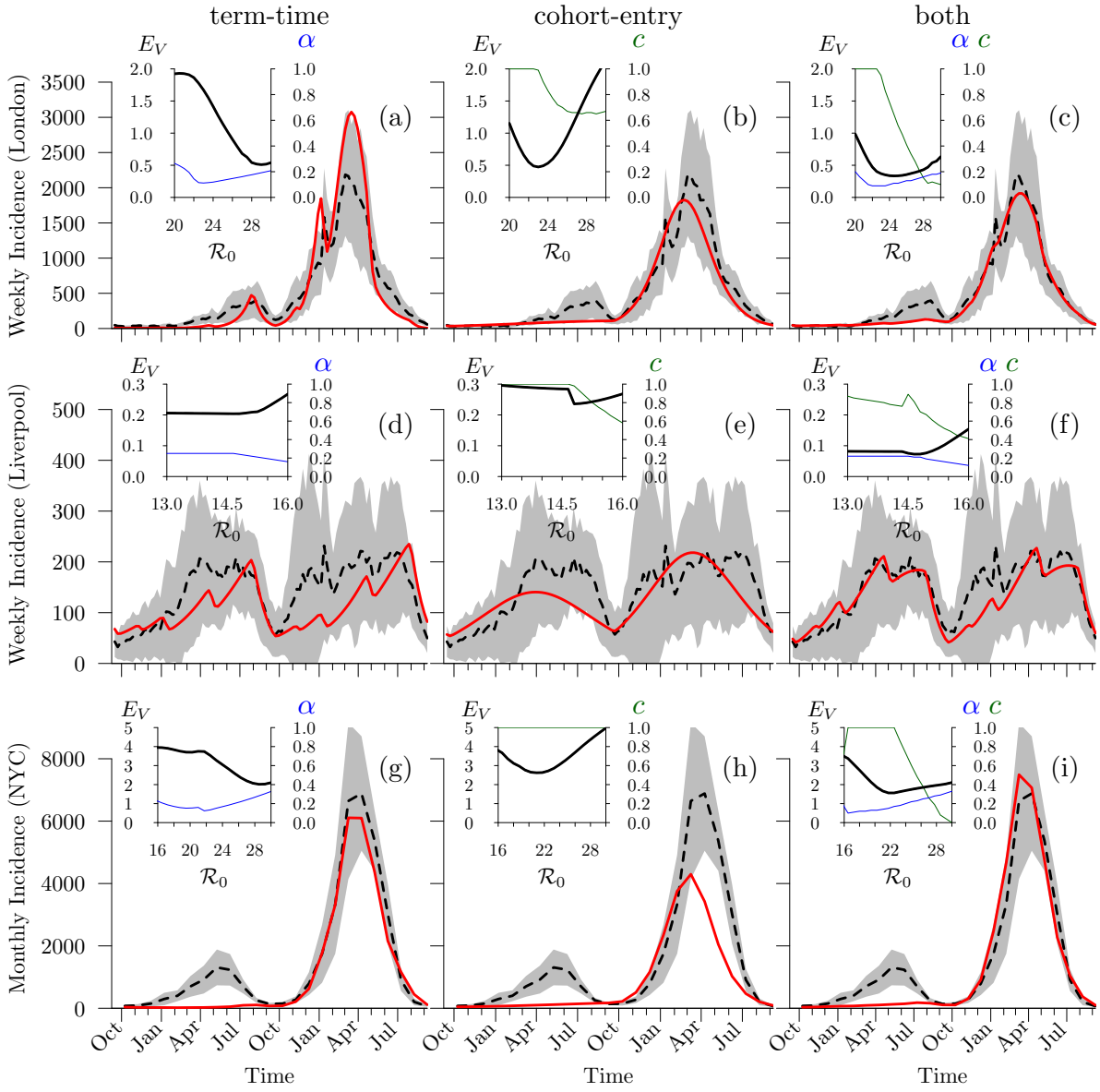

Figure S4: Fitting models by trajectory matching to measles incidence data for three cities (*cf.* **Figure 4** for the equivalent for the aggregated E&W measles data). From top to bottom: London (UK), Liverpool (UK), and New York City (US). From left to right: term-time forcing only, cohort-entry only, and both effects. In all of nine main panels, the black dashed curve shows the observed average measles biennium during the period highlighted with grey shading in **Figure S3**, while the red solid curve shows the fitted model simulation. The estimated parameter values are given in **Table S6**. The inset in each panel shows the fitting error E_V (**equation** (9)) as a function of $\mathcal{R}_0$ (black solid curve) and the estimated term-time forcing amplitude (α, blue) or cohort-entry proportion (c, green). School days in E&W, London, and Liverpool were [7,100] (*i.e.,* from 7th to 100th day of the year), [115,199], [252,300], and [308,356]; while in New York City, school days were [3,48], [58,102], [114,179], and [251,357] [14].

7 Parameter estimates and fitting errors

Table S6 shows our best-fit parameter estimates and associated fitting errors for the fits of the various models to the measles biennium in the locations we studied. In all places, including the cohort effect substantially reduces the fitting error (E_V, §**2.3.4**). In addition, the differences in AIC allow us to infer that these improvements are significant.

Table S6: Parameter estimates obtained by fitting epidemic models to measles notification time series in four locations. Parameters that are not fitted are indicated with '–'.

Place	Model	c	α	$\mathcal{R}_0$	η	E_V	ΔAIC
E&W (UK)	term-time (fixed $\mathcal{R}_0 = 17$)	–	0.25	–	0.25	2.867	270.4
	term-time	–	0.15	22.6	0.44	0.813	58.7
	cohort-entry	1.00	–	17.2	0.43	0.732	50.3
	both	1.00	0.16	17.1	0.49	0.229	0.0
	RAS	–	–	13.4*	0.61	0.486	24.7
London (UK)	term-time	–	0.19	29.0	0.41	0.510	16.3
	cohort-entry	1.00	–	22.9	0.40	0.473	12.5
	both	0.65	0.11	24.5	0.42	0.334	0.0
Liverpool (UK)	term-time	–	0.24	14.9	0.40	0.201	11.3
	cohort-entry	0.98	–	14.8	0.45	0.236	15.0
	both	0.81	0.21	14.6	0.47	0.073	0.0
NYC (US)	term-time	–	0.28	28.5	0.10	2.017	45.3
	cohort-entry	1.00	–	21.2	0.07	2.611	107.1
	both	1.00	0.17	22.5	0.11	1.562	0.0

* For the RAS model, $\mathcal{R}_0$ was estimated as the mean of the reconstruction in **Figure 2**. The fitted RAS parameters are b_0, b_2 and η; see **Table S5**.

For England and Wales as a whole and for New York City, the best-fit cohort proportion is $c = 1$. Consequently, a further model selection step could be performed, fitting reduced models in which c and α are each equal to 0 or 1. However, this step would not change which model is selected.

For all the models we considered, finding the best-fit parameters listed in **Table S6** uniquely determined a solution, because there was always a unique biennial attractor for the best-fit parameter values. (Coexisting stable cycles do exist for the cohort model [12, Figures 3.8 and 3.9, p 73], but we have found no evidence of coexisting, distinct biennial attractors.) The proportion susceptible, $S(0)$, at the start of the fitted biennial cycle, is listed for each model in **Table S7**.

Table S7: Initial susceptible proportion $S(0)$ from trajectories fitted to E&W measles. If the system were in equilibrium then the proportion susceptible would be $1/\mathcal{R}_0$.

Model	$\mathcal{R}_0$	$1/\mathcal{R}_0$	$S(0)$
Term-time SEIR	17 (fixed)	0.059	0.053
Term-time SEIR	22.6	0.044	0.037
Cohort-entry SEIR	17.2	0.058	0.063
Both	17.1	0.058	0.062
RAS	13.4	0.075	0.067

8 Dynamical structure in the (α, c) plane with different $\mathcal{R}_0$

Figure 5(d) summarizes the key features of the dynamical structure of the cohort entry SEIR model with term-time forcing for the specific basic reproduction number $\mathcal{R}_0 = 17$. **Figure S5** shows the same information for other values of $\mathcal{R}_0$.

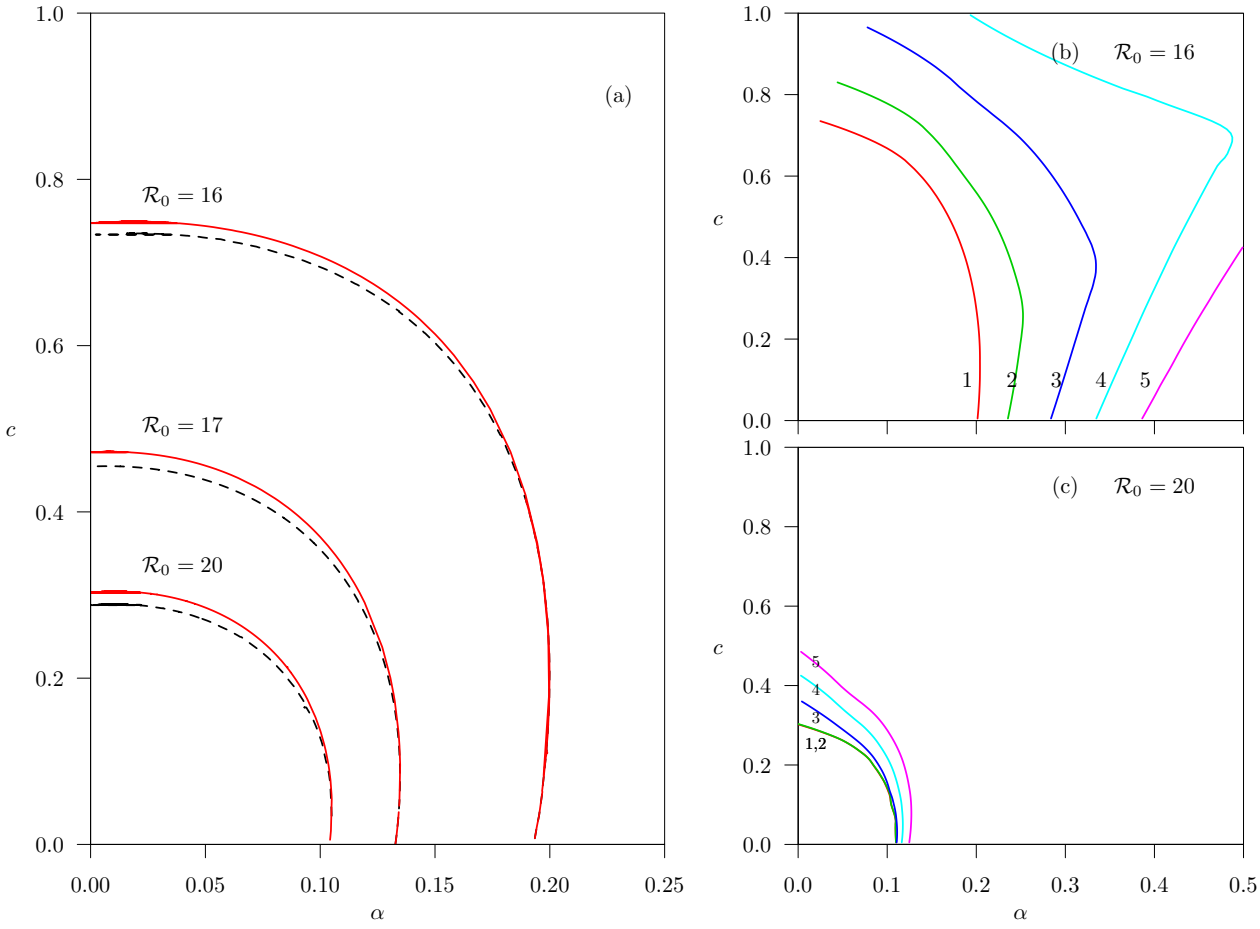

Figure S5: The period-doubling (from annual to biennial) bifurcation curve in the two-dimensional parameter plane (term-time forcing amplitude α *versus* cohort proportion c) with different $\mathcal{R}_0$. (a) The red solid curves show the case of cohort forcing on both birth and death terms, while the black dash curves show the case of cohort forcing on birth term only (*cf.* §3). Panels (b) and (c) show the peak height ratio contour curve associated with biennial cycles for (b) $\mathcal{R}_0 = 16$ and (c) $\mathcal{R}_0 = 20$. The five contour curves in each panel correspond to peak height ratio (major year over minor year) of 1 to 5 as in **Figure 5**(d).

9 Transient dynamics of the cohort entry SEIR model

As mentioned in §3.3, in addition to the topological invariance of the principal bifurcation tree (which summarizes the asymptotic dynamics of the model), the transient dynamics of the cohort-entry model are also qualitatively identical to those of the term-time forced model. **Figure S6** shows the period of the transient oscillations that damp out on a stable annual or biennial cycle in the term-time SEIR model (a) and the cohort entry SEIR model (b).

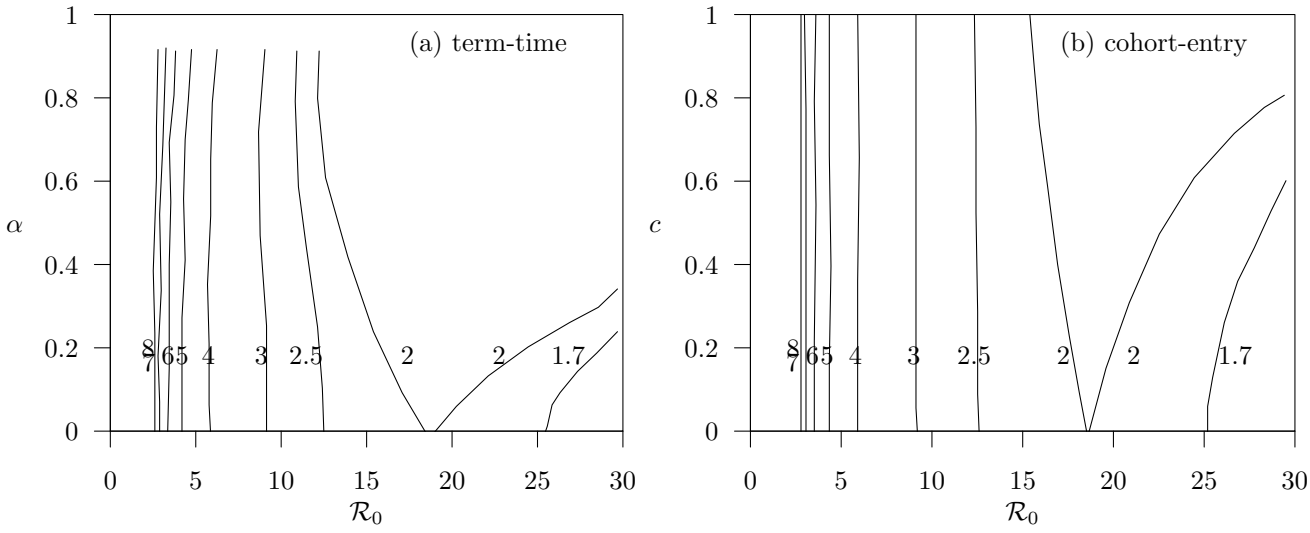

Figure S6: A comparison of contour plots of constant natural damping frequency $T_{f,1}$ in the parameter planes of transmission rate seasonality α versus $\mathcal{R}_0$ for the time-time SEIR model (a) and cohort entry proportion c versus $\mathcal{R}_0$ for the cohort-entry SEIR model (b). The natural damping period contour curves $T_{f,1} = 1.7$, 2, 2.5, 3, 4, 5, 6, 7, and 8 years are shown in both panels; between the two $T_{f,1} = 2$ curves there is a $T_{f,1} = 2$ phase-locked region. Panel (a) reproduces Figure 1a of [10].

References

[1] London, W, Yorke, JA (1973) Recurrent outbreaks of measles, chickenpox and mumps. I. Seasonal variation in contact rates. *American Journal of Epidemiology* 98:453–468.

[2] Yorke, JA, London, W (1973) Recurrent outbreaks of measles, chickenpox and mumps. ii. systematic differences in contact rates and stochastic effects. *American Journal of Epidemiology* 98:468–482.

[3] Hempel, K, Earn, DJD (2015) A century of transitions in New York City's measles dynamics. *Journal of the Royal Society Interface* 12:20150024.

[4] Schenzle, D (1984) An age-structured model of pre- and post-vaccination measles transmission. *IMA Journal of Mathematics Applied in Medicine and Biology* 1:169–191.

[5] Bolker, B (1993) Chaos and complexity in measles models: A comparative numerical study. *IMA Journal of Mathematics Applied in Medicine and Biology* 10:83–95.

[6] Bolker, BM, Grenfell, BT (1993) Chaos and biological complexity in measles dynamics. *Proceedings of the Royal Society of London, Series B, Biological Sciences* 251:75–81.

[7] Keeling, MJ, Rohani, P (2008) *Modeling Infectious Diseases in Humans and Animals* (Princeton University Press, Princeton, New Jersey).

[8] He, D, Earn, DJD (2007) Epidemiological effects of seasonal oscillations in birth rates. *Theoretical Population Biology* 72:274–291.

[9] Earn, DJD, Rohani, P, Bolker, BM, Grenfell, BT (2000) A simple model for complex dynamical transitions in epidemics. *Science* 287:667–670.

[10] Bauch, CT, Earn, DJD (2003) in *Dynamical Systems and Their Applications in Biology*, Fields Institute Communications, eds Ruan, S, Wolkowicz, G, Wu, J (American Mathematical Society, Toronto) Vol. 36, pp 33–44.

[11] Earn, DJD (2009) in *Mathematical Biology*, IAS/Park City Mathematics Series, eds Lewis, MA, Chaplain, MAJ, Keener, JP, Maini, PK (American Mathematical Society) Vol. 14, pp 151–186.

[12] He, D (2006) Phd (McMaster University, Canada).

[13] Fine, PEM, Clarkson, JA (1982) Measles in England and Wales — I: an analysis of factors underlying seasonal patterns. *International Journal of Epidemiology* 11:5–14.

[14] Bauch, CT, Earn, DJD (2003) Transients and attractors in epidemics. *Proceedings of the Royal Society of London, Series* B 270:1573–1578.